The breaking and remaking of a bond: Caging of I_2 in solid Kr

R. Zadoyan, Z. Li, C. C. Martens, and V. A. Apkarian
Department of Chemistry, University of California, Irvine, California 92717

(Received 29 June 1994; accepted 6 July 1994)

The caging of I_2 in solid Kr is followed in real-time following its dissociative excitation on the $A(^3\Pi_{1u})$ surface. The experiments involve pump–probe measurements with a time resolution of $\geqslant$150 fs. The experimental signals are reproduced using classical molecular dynamics simulations, and the classical Franck approximation. The comparison between experiment and simulation allows an unambiguous interpretation of features in the observed signal as being due to the initial impulsive stretch of the I–I bond, collision of the atoms with the cage wall, recoil and recombination, and the subsequent coherent oscillations of the nascent I_2 molecule. These detailed observations are possible due to retention of coherence along the I–I coordinate throughout the caging process. The extent of coherence is dictated mainly by the initial impact parameters of the molecule-cage collision, which in turn is controlled by the thermal and zero-point amplitudes of lattice vibrations. The caging is well-described as a sudden process, involving a binary collision between I and Kr atoms with nearly complete energy loss of the I atom upon completion of the first collision. Vibrational relaxation of the bound molecule proceeds on the time scale of 12 ps. The nontrivial relation between this relaxation time and decay rates that may be extracted from experimental transients is discussed. Although the interplay between the nested A and A' potentials is not detectable, it is clear that in the studied range of initial excess energies, 1000–1700 cm^{-1}, the recombination remains effectively adiabatic, and does not involve the ground state.

I. INTRODUCTION

Ever since the introduction of the concept by Franck and Rabinowitch,[1] the "cage effect" has played a central role in studies of reactive photodynamics in condensed media. The process has been investigated in photodissociation studies of small molecules isolated in van der Waals solids and clusters by time-independent experiments and by molecular dynamics simulations.[2] A very large literature on the subject has also been devoted to liquid phase[3] and high pressure[4] studies. More recently, the investigations have been extended to the realm of femtosecond time-resolved measurements in clusters,[5,6] in liquids,[7–9] and in high pressure gas.[10] From the first definition of the process as a realization of a condensed phase effect in reactive dynamics,[1] up to the most recent time resolved measurements,[3,4,6,7,10] the photodissociation recombination of I_2 remains the most intensively investigated prototype in these studies. Without reviewing this very large body of work, it is possible to assert that nearly all of the observations to date relate to the cage *effect*—namely, observation of the *consequences* of caging, and not the caging process itself. The disappearance of optically prepared reagent states, and the reappearance of the molecular states as recombination products are the usual observables. In our first published study of the caging of I_2 in solid Ar, we demonstrated that the caging *process* itself could be followed in real-time in its entirety, without any discontinuity in observables.[11] In this paper we extend those studies to I_2 photodissociation recombination in solid Kr.

The aim of photodynamical studies on small molecules isolated in rare gas solids is to provide a first principles understanding of many-body interactions which, in turn, is the underlying challenge of condensed phase reactive dynamics in general. With the advent of femtosecond lasers, it is now possible to prepare superposition states in condensed media that are sufficiently localized to allow the definition and detection of elementary microscopic events in space and time. With proper choice of systems, pump–probe measurements with short pulses allow the interrogation of evolving dynamics far removed from the vertically accessible Franck–Condon region, hence configurations and time scales relevant to chemical change become accessible. In addition, to providing the possibility of directly observing reaction progress in condensed media, these tools promise the possibility of intervention in the course of a chemical reaction. Several examples from the recent literature illustrate these contentions. We have previously reported the direct observation of bond formation in the liquid phase between Xe^+Cl^- and solvent Xe to form $Xe_2^+Cl^-$, and have shown that the normal progress of the reaction could be suppressed by stimulating the radiative dissociation of the Xe^+Cl^- intermediate.[12] The sudden photodissociation of I_3^- (Refs. 9, 13, and 14) and HgI_2 (Ref. 15) have been studied in the liquid phase by monitoring in real time the oscillations of the product fragments, I_2^- and HgI, respectively. The observed oscillatory signal in these cases can be ascribed to the coherent evolution of the suddenly created vibrational superposition on the bound potential of the photofragment. In another example, the liquid phase predissociation of $I_2(B)$ has been followed by monitoring the reaction coordinate using time-domain transient dichroism, providing a detailed analysis of the origin and persistence of coherences in the solvated molecule.[16] This partial list of experiments is representative of the field of condensed phase time resolved reactive dynamics and the types of information that can be extracted from direct measurements.

There are, at present, several time domain studies in the literature that directly probe caging upon photodissociation.

 0021-9606/94/101(8)/6648/10/$6.00

In contrast with the aforementioned listed examples, these studies are aimed at following motion along a dissociative molecular coordinate—a coordinate along which, at least temporarily, the atomic fragments are held by the solvent alone. Among the first of this genre of investigations is the elegant series of experiments on the cage-induced recombination of I_2^- trapped in size selected clusters of CO_2.[5] These studies have shown that, upon completion of the first solvation shell, recoil of photofragments occurs with little dispersion in time, producing observable oscillations in the recombinant molecular ion. Femtosecond studies of the solvent-induced recombination of I_2 in liquid CCl_4 (Ref. 6) and in Ar clusters[7] studied by pump–probe measurements have shown the signature of prompt recombination events that proceed on the time scale of ~500 fs. A similar conclusion was inferred in studies of CH_2I_2 in liquids, in which the observed initial 350 fs decay of a transient absorption was ascribed to loss of CH_2I by direct geminate recombination.[8] For neutral I_2 in liquids and size-unresolved clusters, in which caging is not complete, recombination arising from various channels ranging from single collision events to diffusion-controlled cage reentry contribute to the observed signals. Accordingly, while a prompt initial edge of the transients may be identifiable, the dispersion in recombination times precludes the retention of coherence in the population of the reformed molecule. In the absence of well-identified resonances, the interpretation of these transients is somewhat speculative. In contrast, in van der Waals solids at low excess energies, conditions can be chosen to insure that caging is complete.[1] In effect, solid matrices provide the possibility of isolating the direct recombination channel. Furthermore, the structural disorder inherent in liquids and the size distributions of small neutral clusters are eliminated. As a result, sharper spatial and temporal resolution of the observable molecular dynamics is to be expected, observables that would be expected to be amenable to direct interpretations. These expectations were realized in the first time-resolved study of photodissociation in matrices, I_2 in solid Ar, which we recently reported together with theoretical simulations.[11] With the present extension to solid Kr, besides reinforcing some of the earlier conclusions, a deeper understanding of the experiment and the underlying molecular physics is sought.

We show that, notwithstanding the approximate nature of the employed potentials, the pump–probe measurements in Kr are amenable to unambiguous interpretation by a nearly quantitative reproduction of the experimental transients through simulations. By performing temperature and wavelength dependent studies, it is possible to uniquely identify features in the experimental transients corresponding to the extension of the I–I bond, the collision of the atoms with the host cage, the recoil of fragments, and the subsequent oscillations of the nascent molecule. These details are observable because the transition dipoles involved in the pump and probe transitions remain localized on the I_2 bond, and the motion along the I–I coordinate retains partial coherence throughout the process. The extent of this coherence we infer to be dictated mainly by initial impact parameters, which in the cryogenic matrix is mainly controlled by the amplitude of zero-point fluctuations of the lattice. The analysis also establishes the molecular configurations involved in the pump and probe resonances, which, although necessary inputs for the unique interpretation of data, are commonly lacking in condensed phase time-resolved studies.

We also show that the experimental observables are well reproduced by classical simulations, combined with the classical Franck principle to reconstruct the pump–probe signals from ensembles of trajectories. This approach can be justified in advance. General formalisms have been given in the literature for the theoretical construction of ultrafast pump–probe signals.[17–20] It is firstly recognized that when an excited state is prepared with an ultrashort pump pulse, a wave packet is created whose center evolves approximately according to classical mechanics.[21] When the pump pulse is so short that its transform is broader than the thermal absorption band of the particular transition, then a Gaussian wave packet, a copy of the ground state configuration distribution, is created on the excited surface. For pulses that are longer in time and, in particular, when they are longer than recursion periods in the ground state, exact time propagators of the interaction Hamiltonian need be used to describe the state prepared by the radiation field.[17–20] In essence, the time evolution of the prepared state on the excited electronic state, the hole created in the nuclear density function of the electronic ground state, and their coupling through the radiation field, need to be taken into account. This consideration is relaxed at cryogenic temperatures where the energy of the system is much smaller than the inverse pulse duration, $k_B T \ll \hbar/\tau_1$, and only $v=0$ of the molecular ground state is populated.[20] In this case, a time evolving hole in the ground electronic state can only be created by stimulated Raman processes—a second order effect in the radiation field, which can be ignored under the weak field excitation conditions of the present experiments. It has also been recognized that when the initially created wave packet is probed by ultrashort pulses that are not phase locked to the pump pulse, then the observed signal is insensitive to the quantum coherence (i.e., the internal phase structure of the packet) of the evolving state, but rather reflects its classical motion.[18,19] This can be understood by noting that as long as the probe pulse duration is shorter than dynamical recursions in either of the electronic states involved in the probe transition, then the boundary conditions that determine the wave functions of the nuclear eigenstates are not sampled, and the instantaneous nuclear superposition states can be treated as if on free potential surfaces. Conservation of atomic positions and momenta remain the constraints during the electronic probe transition; accordingly, the transition probability is simply given by the probability that the evolving packet reaches a configuration where the difference in potential energies of the electronic states involved in the probe transition equals the probe laser energy: $h\nu_{\text{probe}}=\Delta V$. This is simply a restatement of the classical Franck principle for absorption.[22] This consideration will be generally applicable for both pump and probe transitions in cryogenic solids, given that short pulses and weak fields are used. It is worth noting that the requirement of ultrashort probe pulses is generally relaxed in condensed media for transitions that involve structureless absorption

spectra, where coherences are strongly damped by the large number of coupled degrees of freedom.

The required inputs for the analysis of the observables, and the underlying dynamics, are the many-body potentials of the different electronic states involved in pump and probe transitions. These are generally not known. In fact, understanding dynamics in condensed media is equivalent to understanding the many-body potentials. Starting with approximate surfaces, iterations between experiment and simulation is perhaps the only viable method for obtaining reliable descriptions of such hypersurfaces, and equivalently, for providing a detailed description of the relevant many-body dynamics. The usual starting point of such an iterative process is to construct surfaces using pair potentials, under the assumption of pairwise additivity. In the case of open shell fragments, a somewhat more sophisticated approach is necessary. Adiabatic surfaces may be constructed by taking proper account of quantization axes, as already shown for I and O atoms in rare gas solids.[23,24] Dynamics including nonadiabatic processes can then be treated systematically by various approaches, first examples of which have been provided in the treatment of photodissociation of HCl and Cl_2 (Ref. 25) and, more recently, in the case of photomobility of F atoms (Ref. 26) in rare gas solids. Here, we rely on a simpler construct with the aims of providing a clear interpretation of observables and clear insights into the main dynamical implications. We carry out classical simulations on a single surface using approximate pair potentials for I–Kr and Kr–Kr interactions. We then rely on one-dimensional effective solvated potentials for the simulation of the signals. With some care, we show that an almost quantitative reconstruction of the pump–probe signals can be derived by assignments of the resonances that are consistent with the potentials used.

II. EXPERIMENT

The experimental approach, which we briefly describe here, is nearly identical to those previously reported.[11] I_2 doped Kr films are prepared by spraying the premixed gas sample on a cold window. The gas composition is typically 1:5000, the film thickness is of order 20 μm, and the base temperature of the sample is 15 K. Deposition conditions are adjusted to produce optically transparent films. In optically scattering films, the pump–probe response time can stretch to many picoseconds due to photon diffusion in the sample. The cracking of the solid upon thermal cycling is usually sufficient to destroy the time response. Accordingly, the choices of deposition and experimentation temperatures are somewhat limited. A second requirement in the sample preparation is the verification that I_2 is isolated as monomers in the solid. This is established via resonant Raman spectroscopy. Resonant Raman spectroscopy is a rather sensitive tool for this purpose since the 212 cm^{-1} fundamental frequency of the monomer is reduced to 180 cm^{-1} in dimers and larger clusters.[27] The preparation conditions are adjusted to completely eliminate cluster signals.

A pump laser, operating between 736 and 700 nm, prepares mostly $I_2(A)$ on its repulsive wall, 1000–1700 cm^{-1} above the dissociation limit of the free molecule. The second harmonic of the pump laser is used to probe the prepared state via laser induced fluorescence from the ion-pair states of I_2. A schematic of the experimental setup is shown in Fig. 1. The cross correlation between pump and probe beams, obtained by difference generation in a 0.2 mm β-BaB_2O_4 (BBO) crystal, is recorded simultaneously with the fluorescence signal from the sample. With this arrangement, the response function of the system is ~180 fs [full width at half maximum (FWHM) of cross correlation]. At the expense of losing the simultaneous record of signal and cross correlation, when the pump and probe pulses are made nearly collinear, the time response of the system is reduced to 150 fs. This is discerned from the experimental data, which contain a response limited initial resonance (see the following). The origin of time, $t=0$, remains ill defined in these experiments due to additive dispersion between sample and cross correlator.[11]

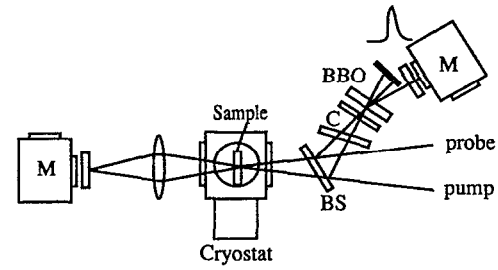

FIG. 1. Experimental diagram. Using a beam splitter (BS), the pump and probe pulses are overlapped on the sample and the difference generation crystal (BBO), simultaneously. Dispersion compensators (C) are added to match the dispersion due to optical elements between the two legs. Fluorescence from the sample is collected through a 0.75 m monochromator (M), after passing it through a bandpass filter. The difference frequency generated at the cross correlator is filtered and detected through a 0.25 m monochromator (M).

III. SOLVATED POTENTIALS

The potential energy curves relevant to the present studies are shown in Fig. 2(a). The vibrationally relaxed ion-pair emission, which in Kr occurs at 420 nm and shows a radiative lifetime of 20 ns, is monitored in the experiments. The parentage of this emission has previously been assigned to the molecular $D' \rightarrow A'$ transition, albeit that it is red shifted from its gas phase origin by ~0.7 eV.[28] The molecular ion-pair states can be expected to be most strongly perturbed by the matrix environment. Besides solvation by polarization of the medium, contributions from the $Kr^+I_2^-$ charge transfer configuration and $I^-(Kr^+I)$ configuration in which a diatomic fragment isoelectronic with IBr appears, undoubtedly contribute to this shift. In fact, the emission spectra which occur from the ionic states after lattice relaxation are rather broad and cannot be interpreted without inclusion of contributions from I–Kr coordinates. Despite these considerations, a satisfactory interpretation of the experimental data is derived by the implicit assumption that the excitation remains localized on the I–I bond. It is reasonable to assume that the six lowest ion-pair states that correlate with $I^+(^3P)+I^-(^1S)$, and which exhibit very similar energetics in the gas phase, are overlapped and strongly interacting in the solid state, producing a

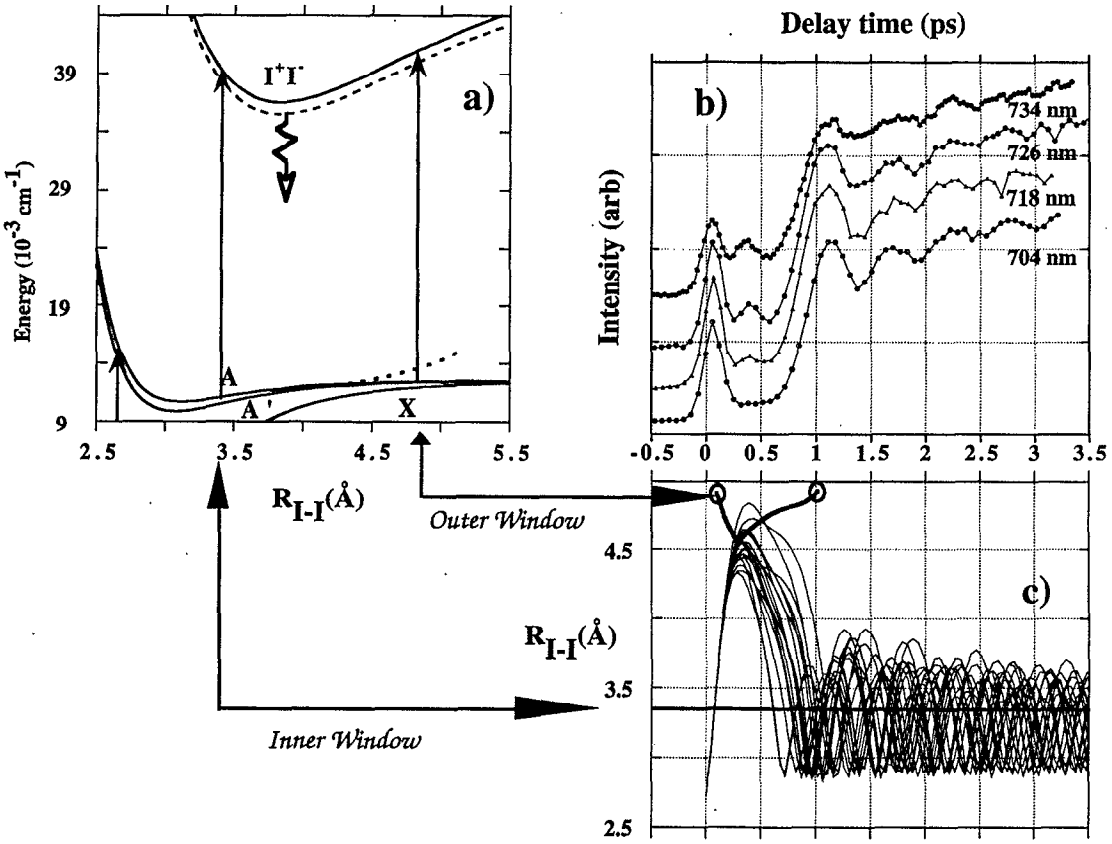

FIG. 2. (a) Partial potential curves of I_2 isolated in solid Kr. The bare A, A', and the *sudden cage wall* (dotted line) are the states on which the dynamics evolves. The probe resonance reaches the vertically accessible ion-pair states, and the detected signal corresponds to fluorescence from these states after lattice relaxation (dotted curve). For a given excitation (726 nm indicated), two molecular configurations are probed: the outer window corresponds to a collision induced resonance at the cage wall. (b) The experimental laser induced fluorescence intensity is displayed as a function of delay between pump and probe lasers. The pump wavelengths are indicated, the probe wavelength in each case corresponds to second harmonic of the pump. (c) Simulated internuclear separation of I_2 as a function of time for 20 representative trajectories (T=45 K). Here, the inner probe window corresponds to the horizontal line. The outer resonance is created in this plane upon dilation of the cage, its location along the I–I coordinate evolves in time, as illustrated schematically by the curved line. The different features of the signals can be identified by following the vertical gridlines down to the simulation box, and noting the crossings of the trajectories with the horizontal resonance lines.

structureless absorption band. As a result, and as already established in the case of I_2 in solid Ar,[11] at a given probe wavelength both A and A' electronic states are interrogated via $\beta(1_g)\leftarrow A(1_u)$ and $D'(2_g)\leftarrow A'(2_u)$ covalent to ion-pair contributions. In the Ar studies, it was discovered that a consistent interpretation of the observed resonances could be given when representing the solvated ion-pair potential by the Rittner form of the gas phase D' potential,[20] after vertically lowering it to reproduce the red shift, and after stretching its equilibrium distance by 0.2 Å. The same applies in the present case. Analysis of the pump–probe signals allows the location of the vertically accessed ion-pair states relative to the assumed A state potential (r_e=3.8 Å and T_e=36500 cm^{-1}). To account for the emission peak from these states, a Stokes shift of 0.125 eV is required. The latter can be ascribed to the stabilization of the ion-pair states by lattice relaxation, and partial charge delocalization.

Information concerning the matrix isolated A and A' states comes mainly from the vibrationally relaxed emission spectra.[28,30] At least near the bottom of these potentials, the matrix perturbations are minor. Taking the matrix shift in electronic origins into account while maintaining the gas phase $I(^2P_{3/2})+I(^2P_{3/2})$ asymptotic limit, these curves are represented in Fig. 2(a) by Morse functions. The difference potential between the bare A/A' and the solvated ion-pair state is double valued. Accordingly, at a given probe wavelength, two molecular configurations are interrogated simultaneously. These are identified as the *inner* and *outer* probe windows in Fig. 2. The location of the outer window requires a more subtle consideration. It occurs far enough out on the attractive limb of the I_2 potential to be strongly affected by the I–Kr interactions. Since this resonance depends explicitly on I–Kr coordinates, it cannot be strictly located in a one dimensional potential energy plot. To see this more clearly, consider the case of a rigid Kr lattice. Upon stretching the I–I bond, the *sudden cage wall* resulting from the repulsive I–Kr interactions will be encountered. This is shown in Fig. 2(a) by the dashed curve, using Lennard-Jones pair potentials to describe the I–Kr interactions. Since the *sudden cage wall* is significantly more repulsive than the Coulombic potential

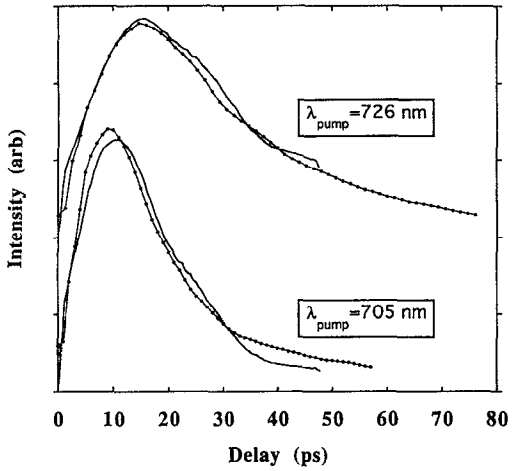

FIG. 3. Experimental signals at long-time (dotted curves) obtained with pump wavelengths of 705 and 726 nm, and the simulated signals for inner resonance windows at $R=3.39$ and 3.31 Å, respectively.

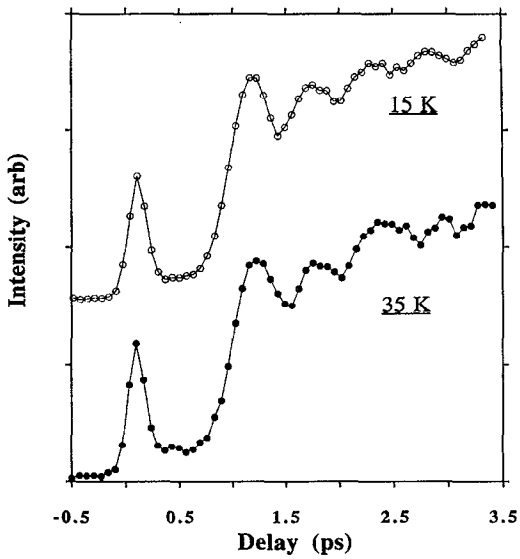

FIG. 4. Temperature dependence of transients for experimental temperatures of 15 and 35 K, recorded with a pump wavelength of 704 nm. The measured signals are observed to be insensitive to temperature.

which describes the attractive limb of the ion-pair states, the outer resonance window disappears. However, upon absorbing the collision impact from I atoms, the Kr cage should dilate, moving the cage wall further out. As the Kr atoms are set into motion, the potential energy along the I–I coordinate drops somewhere between the *sudden wall* value and the bare I–I potential. Thus the occurrence of the outer window resonance depends intimately on the atom-cage collision dynamics, and may be regarded as a *collision-induced absorption.*

Note that there is little independent information about these solvated potentials. The time-resolved experiments, along with simulations, should provide refinements of these interactions, especially at the stretched molecular configurations which cannot be interrogated by frequency domain measurements alone.

IV. EXPERIMENTAL RESULTS

The time profiles of the pump–probe signals obtained at four different wavelengths are shown in Fig. 2(b). Clear oscillations are observed in these signals. After an initial response-limited peak in time, the main recurrence in the signal appears at a delay of ~1 ps; the subsequent oscillations have a period of ~0.5 ps and persist for delay times of several picoseconds. The most noticeable trend in the wavelength dependence is the appearance of a peak at a delay of ~400 fs, which gains in prominence as the wavelength is increased. With the aid of molecular dynamics simulations, this portion of the signal can be unambiguously assigned to the resonance at the outer window. After the first ~5 ps, the experimental transients evolve smoothly. They develop a maximum and then decay to the baseline on a timescale that is determined by the probe wavelength. This is illustrated in Fig. 3, in which the long-time behavior of transients obtained at two different wavelengths are shown. When the decays are fitted to single exponentials, fall times of 25 and 9 ps are obtained from the transients at probe wavelengths of 353 and 363 nm, respectively. These decay times show a weak dependence on temperature. Between 18 and 50 K, the decay time of the 726 nm transient reduces from 9 s to 7 ps. The early time evolution of the pump–probe signal is virtually independent of temperature, as illustrated in Fig. 4.

V. SIMULATIONS

Classical simulations are carried out on a single I_2 molecule occupying a double substitutional site of the Kr lattice. The lattice is represented by 500 Kr atoms, using periodic boundary conditions. All interactions are assumed to be pairwise additive. The I–I interaction is represented by a single Morse potential: $D_e=12\,550$ cm^{-1}, $r_e=2.65$ Å, and $\beta=1.871$ Å^{-1} for the X state, and $D_e=1840$ cm^{-1}, $r_e=3.10$ Å, and $\beta=2.147$ Å^{-1} for the A state. The I–Kr interaction is represented by Xe–Kr Lennard-Jones parameters: $\sigma=3.74$ Å, $\epsilon=233.5$ K. Lennard-Jones potentials are used for the Kr–Kr interactions as well: $\sigma=3.58$ Å, $\epsilon=199.9$ K. The system is first equilibrated at a prespecified temperature using the $I_2(X)$ state parameters. Initial configurations are randomly chosen from the equilibrated set with the condition that $R(I_2)$ correspond to the desired Franck–Condon resonance condition within the energy bandwidth of the excitation pulse. The $I_2(X)$ potential is then suddenly switched to $I_2(A)$, and Hamilton's equations are propagated in time.

The resulting time dependence of the I_2 separation for a representative ensemble of trajectories is shown in Fig. 2(c) below the experimental transients. The ensemble starts at $r\sim2.6$ Å, the equilibrium distance on the X state. The I–I bond stretches until stopped by collision with the cage atoms. The observed recoil distances are 4.6 ± 0.2 Å. The sudden wall at the same initial excess energy is at 4.6 Å. The dispersion in recoil distances is quite comparable to the rms amplitude of the fluctuations in position of the lattice atoms of 0.18 Å. In essence, the caging of the molecule in solid Kr

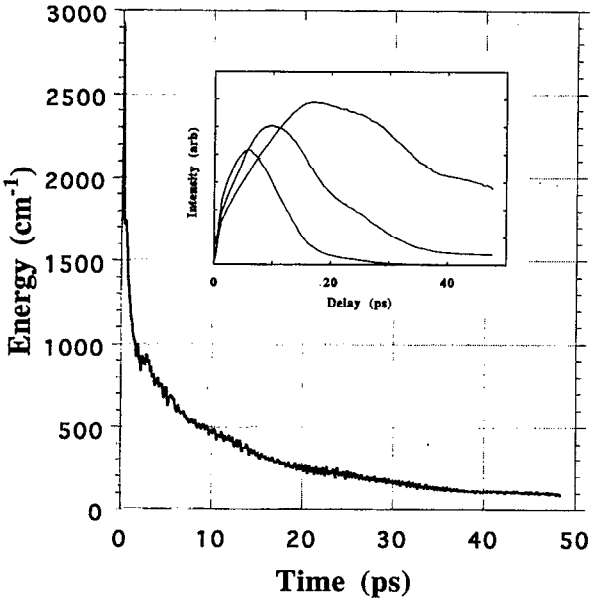

FIG. 5. Ensemble averaged total I_2 energy as a function of time. Fitting the data past the first 5 ps to an exponential yields a fall time of 12 ps. In the inset, the observable pump–probe signal based on the same trajectory ensemble is shown. The signal is constructed for inner window locations at (a) 3.5 Å; (b) 3.4 Å; (c) 3.3 Å.

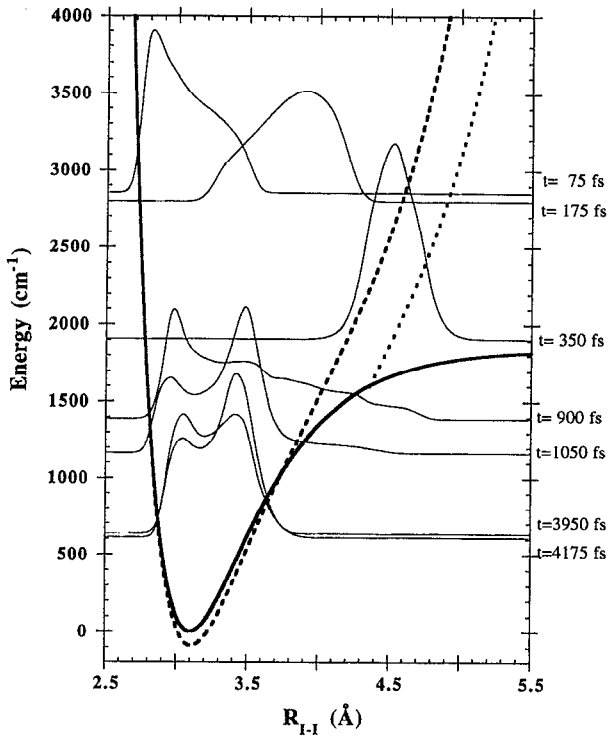

FIG. 6. Wave packets constructed from the classical trajectory ensemble is shown for selected times. The origin of time is taken as the right edge of the laser pulse. The packets are constructed from the Gaussian swarm, after convolution with a laser pulse of 100 fs FWHM. Also shown are the bare I_2 potential, the pair potential used in the simulations, and the sudden potential, computed by freezing the lattice in its equilibrium position. The collision with the wall is complete at $t\sim350$ fs, at which point the packet has lost nearly all of its excess kinetic energy and has been focused behind the rigid wall. The wall has been pushed out, and the new position is inferred from the centroid of the packet and indicated by the dotted line.

can be regarded as a sudden process. This conclusion is further reinforced by inspection of the time dependence of the ensemble averaged total I_2 energy, which is illustrated in Fig. 5. For the initial ~4 ps, the energy loss occurs in a stepwise manner, due to well defined binary collisions between the coherently evolving ensemble of I_2 fragments and the host lattice. At longer times, the decay becomes nearly exponential with a time constant of 12 ps. This relaxation is due to many weak and uncorrelated collisions between the I atoms and the Kr host.

The results of the classical molecular dynamics simulations are also summarized by the alternative, wavepacket representation in Fig. 6. These are constructed from an ensemble of 200 trajectories, by replacing the classical positions with Gaussians, and then convoluting them with a laser pulse of 100 fs FWHM. For the Gaussians, the square of the A state harmonic vibrational ground state is used. The instantaneous wave packets are then plotted vs the ensemble average energy of Fig. 5. Also shown in Fig. 6 are the bare $I_2(A)$ potential, and the same potential including the I–Kr interactions for a rigid lattice at equilibrium (the sudden wall). We highlight several aspects of the results that are discernible from the figure. Upon termination of the 100 fs irradiation pulse, the packet spread is ~1 Å, and the system immediately starts to lose energy. The collision of the packet with the cage wall is completed at $t\sim350$ fs, at which point nearly all of the initial kinetic energy is dissipated. The complete energy loss is in accord with the description of a binary, head-on collision of the I atoms with stationary Kr atoms, for which an energy loss $\Delta E/E=4m_I m_{Kr}/(m_I+m_{Kr})^2=0.96$ can be expected. The collision stops the wave packet, with some focusing, past the sudden wall location. In effect, the cage wall has been pushed out, and the inferred new wall location is indicated by the dotted curve. The recoil and recombination occur with significant spreading of the packet. At $t=900$ fs, the packet is already in the bound part of the molecular potential yet it is spread over ~2 Å along the I–I coordinate. The recombination time is longer than a vibrational period. At $t=1050$ fs, after compression of the I–I bond the packet has already returned to the right turning point of the potential. Nevertheless, a fraction of the population remains outside. This slow filling rate limits the extent of coherence in subsequent vibrations of the reformed bond. The extent of vibrational coherence retained is illustrated by the two packets near $t\sim4$ ps. These show that the spread in phase space is not complete, and that approximately 5% of the population oscillates between turning points. This time evolving distribution is a measure of the partial coherence in the vibrational motion of the newly formed bond, and is the origin of the observable oscillatory signal in the pump–probe measurements.

VI. DISCUSSION

The main features of the observed signals are directly interpretable on the basis of the classical molecular dynamics

simulations, with guidance from the classical Franck principle: optical excitation is a vertical process which occurs at atomic configurations for which $\Delta V(R)=V_{D'}(R)-V_A(R)=h\nu_{\text{probe}}$. For such an interpretation, if we constrain ourselves to the one-dimensional potential curves of Fig. 2(a), it is sufficient to identify the I–I internuclear separations that lead to the resonance condition. To a good approximation this is possible in the case of the inner window resonance, the location of which we expect to be only mildly modulated by the Kr coordinates. For a pump wavelength of 726 nm, and a probe wavelength of 363 nm, based on the potentials of Fig. 2(a), the inner window can be located at $R_{\text{I-I}}=3.3$ Å. The crossings of the trajectories with the horizontal line placed at this internuclear distance then correspond to fulfillment of the resonance condition. Inspection of Fig. 2(c) shows that the first crossing occurs with the inner window prior to dispersion of the trajectories, at a delay of 60 fs. This gives rise to the response-limited first peak in the signal [in Fig. 2(b)]. The first recursion at the inner window occurs ~1 ps later, after collision with the cage atoms and recoil. This can be clearly identified with the broadened maximum at $t\sim1.1$ ps in the data. Subsequent crossings of the inner resonance, due to oscillations of the newly formed bond, are responsible for the modulation of the signal which lasts up to ~4 ps.

By following the vertical gridlines in Figs. 2(b) and 2(c), the features in the experimental signals can be related to those of the trajectory ensemble. This makes it clear that the wavelength dependent peak at ~400 fs is due to the collision induced resonance at the outer window. This contribution to the signal occurs in time at the first turning point of the trajectories. In this one-dimensional representation, the resonance condition for the outer window may be represented by crossings of the trajectories with a *time-dependent* curve corresponding to the locus of potential energy differences that equal the probe laser energy. The shape of such a curve depends on the difference potential between the ion pair and covalent hypersurfaces, and will be specific to each trajectory, since the resonance depends explicitly on motion along the Kr coordinates. A schematic of such a projection is shown in Fig. 2(c). While the exact shape of this curve cannot be determined without a knowledge of the explicit dependence of both covalent and ionic surfaces on I–Kr coordinates, it is clear that the peak at 400 fs is the only contribution of the outer window to the signal. It is this signal that contains a description of the atom-cage collision.

The aforementioned considerations can be put on a more quantitative footing. Given intermolecular separations corresponding to the resonance conditions, it is possible to construct the experimentally observable pump–probe signal from the trajectory ensemble. This is accomplished by convolution of the experimental response function with a sampling function, $S(t)$, which is derived from the ensemble of N trajectories, and is given by

$$S(t)\propto\frac{1}{N}\sum_{j=1}^{2}\frac{|\mu_{if}(R_j)|^2}{|\partial\Delta V(R_j)/\partial R|}\sum_{n=1}^{N}G[R_j^*-R_n(t)]. \quad (1)$$

Here, $G(R)$ is a Gaussian function of R with a spatial width corresponding to $|\psi|^2$ of the A state ground vibrational wave function. The evolving vibrational probability density is thus approximated as a "swarm" of Gaussians centered on each trajectory in the ensemble, and the signal resulting from a probe pulse at time t is the sum of the contributions from each evolving Gaussian evaluated at the two probe windows, weighted by the square dipole moment and a density of states factor.[11] The formulation in terms of the Gaussian swarm avoids the singularities that arise in a purely classical inversion, which was previously used.[11]

Comparisons between simulated and experimental signals are shown in Fig. 3 for the long-time behavior. These signals arise nearly entirely from the inner window resonance, for which the one-dimensional analysis is quite adequate. The experiments are well reproduced by locating the inner window at $r=3.31\pm0.02$ Å for the 705 nm data, and at $r=3.39\pm0.02$ Å for the 726 nm data. The sensitivity of the time profiles of the synthesized signal to the location of the probe resonance window is illustrated in the inset to Fig. 5, in which for the same trajectory ensemble the observable signals are shown for $r=3.3$, 3.4, and 3.5 Å. With the assumption that the energy relaxation of the molecule is being properly reproduced by the classical treatment, these fits fix the inner window location, and locate the repulsive wall of the ion-pair state relative to the assumed A surface.

The dependence of the signal profiles on probe window location, as illustrated in the inset to Fig. 5 raises a rather important point. The decay time obtained by fitting the pump–probe signal, whether measured experimentally or generated by simulation, does not yield the same decay constant as obtained by considering the energy relaxation of the I_2 directly. These decay times should, in fact, not agree in general, as the observable signal results from a subtle interplay between vibrational energy relaxation, spreading of the evolving vibrational energy distribution, and the instantaneous velocity of the trajectory ensemble in the resonance window (or analogously, the dwell time of the quantum wave packet), and not simply the energy relaxation itself. The broad range of *apparent* decay rates that can be extracted from the signals generated using a *single* trajectory ensemble with a well-defined vibrational relaxation time, by changing the position of the probe resonance window (see Fig. 5), clearly indicates the need for caution in the interpretation of ultrafast transients in which the molecular resonances are not established. To the extent that the interaction potentials are realistic, we expect the vibrational relaxation to be well described by the classical simulations, as the spacing among the molecular vibronic states is well within the phonon continuum of the solid, and accordingly the dynamics evolves in a continuum of states.

The comparison between experiment and simulation for the early time evolution is shown in Fig. 7. The simulations are carried out at two different temperatures, 15 and 45 K. The simulated signals in Fig. 7 are based on ensembles of 40 trajectories each. They are synthesized with the inner resonance window fixed from the long time comparison at 3.39 Å. The outer window location is then chosen (at 4.75 Å in the 15 K trajectories, and at 4.8 Å in the 45 K trajectories) to reproduce the peak at a delay of ~400 fs, and the intensity

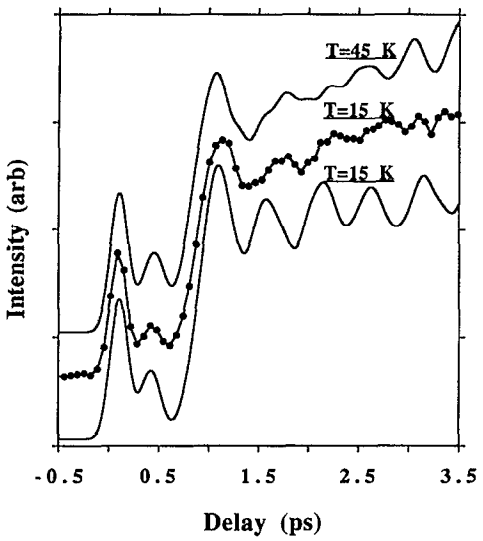

FIG. 7. Comparison between experiment (middle trace) and simulation at 15 K (lower trace) and 45 K (upper trace), for a pump wavelength of 726 nm.

under this peak is adjusted to coincide with the experimental signal. The qualitative features of the experiment are reproduced by the synthesis; this involves a nearly quantitative reproduction of the signal for the first 1.5 ps, the signal envelope out to 3.5 ps, and the oscillation frequency of ~0.5 ps past the main recursion [which is more clearly observed in the 704 nm data of Fig. 2(b)]. The 45 K signal was also synthesized from an expanded set of 200 trajectories. The main difference between the different size ensembles is the detail of the structure in the oscillatory part of the signal between 1.5 and 3.5 ps. At present, we only extract one measure from this part of the signal, namely, the depth of the modulation, which is a measure of the extent of vibrational coherence in the reformed I–I bond. Quite clearly, the depth of modulation in the synthesized transients depends on temperature. In contrast, the experimental transients of Fig. 4 do not show any appreciable temperature dependence. Moreover, the depth of modulation of the 45 K simulation is closer to the 18 K experiment. These results can be understood by considering the role of lattice zero-point motions on the observed coherence.

At the experimental cryogenic temperatures, zero-point energy of the lattice is nearly equal to the thermal energy. As such, in a purely classical simulation, a temperature scaling of classical trajectories is required to reproduce the proper vibrational amplitudes of the lattice. Such a scaling has previously been prescribed for extracting spectra from classical simulations.[31] To match with experiments at temperature T, the classical system is simulated at an artificially elevated temperature T', given by

$$T' = \frac{\hbar\omega}{2k_B}\left[\tan h\left(\frac{\hbar\omega}{2k_B T}\right)\right]^{-1}. \tag{2}$$

The Debye temperature of solid Kr is $\hbar\omega/k = 72$ K.[32] Therefore at $T = 18$ K, a correction factor of $T'/T = 2.1$ is required. Thus the 45 K simulation should be a more realistic representation of the experiments, and indeed yields a rather more satisfactory agreement in the comparison of Fig. 7. The virtual indistinguishability of signals recorded at 15 and 35 K can also be understood in this context. In the studied temperature range, while T is more than doubled, T' changes by only ~20%. Note the implication that the initial distribution in position, which scales as $\sqrt{T'}$, controls the depth of modulation of the signal. This result can be understood if we note that the extent of coherence in the recombinant pair is dictated by the nature of the initial molecule-cage collision and recoil. In that period, the thermal momenta of the lattice atoms are negligible in comparison to the momenta of the photogenerated I atoms and, therefore, of little effect on the outcome of the collision. In contrast, the initial I_2 lattice orientations, which are controlled by thermal and zero-point vibrational amplitudes, dictate the sampling of the impact parameters of the collision and, therefore, cannot be ignored.

While the origin of the wavelength-dependent peak at 400 fs is clear, its reproduction in the synthesized signals of Fig. 7 is somewhat *ad hoc*. In the absence of independent pump and probe lasers and many-body potentials that rigorously describe the collision induced resonance condition, what is learned from this resonance at present is somewhat limited. At an initial excitation of 704 nm the trajectories do not reach the outer window. At 718 nm, they only graze the outer window, which, based on the potentials of Fig. 2(a), occurs near 5 Å. At 726 nm, the resonance due to the outer window gives a well-defined peak, which can be reproduced by the assumption of an outer window fixed at 4.8 Å. To be consistent, in the case of 734 nm excitation an outer resonance fixed at a shorter internuclear distance should be considered. This would force a double crossing with the trajectories. Yet the data do not show any splitting of the 400 fs peak. The absence of such a splitting was further verified by measurements at 726 and 736 nm, in the collinear pump–probe geometry. This is illustrated in Fig. 8. The improved time resolution of this geometry is discerned from the first peak, the inner window resonance, which shows a width of 150 fs (FWHM of the fitted Gaussian). The outer window resonance remains a single peak which can be fitted by a Gaussian of 240 fs FWHM. This a measure of the residence time of the collision induced resonance. The absence of a double crossing at 736 nm is a clear indication that the outer resonance is dictated by the many-body dynamics, and cannot be represented by a fixed window in a one-dimensional analysis. We note that in the case of Ar the equivalent peak clearly splits into two; however, there also it was clear that a one-dimensional analysis could not accurately reproduce the timing of the observed signal.[11] The measurements in Ar have recently been repeated with an improved time resolution, yielding significantly more detail in both the collision induced resonance and the post recoil coherences.

The origin of the post-recoil oscillations are worthy of further comment. Improvement in time resolution from 180 to 150 fs does not produce a significantly deeper modulation of these oscillations in the case of Kr (compare Figs. 4 and 8), while it does in the case of Ar. Here, it is possible to conclude that, despite the fact that the molecule loses nearly all of its excess energy in the first collision with the cage, and nearly a quarter of its vibrational energy during the first

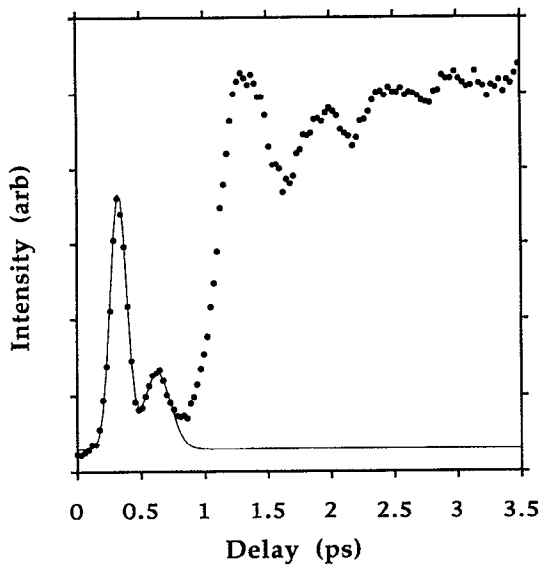

FIG. 8. Time profile of pump–probe signal with collinear geometry (pump wavelength=726 nm). The initial response limited peak is fitted with a Gaussian of FWHM=150 fs, and the peak due to the collision induced resonance, at a delay time of ~400 fs, is fitted with a Gaussian of FWHM =240 fs.

oscillation period in the bound part of the potential (see Fig. 6), the initially created ensemble remains sufficiently localized—in both configuration and phase space—to yield the oscillatory signal for time delays as long as ~4 ps. Despite the extensive loss of excess energy, the *spreading* of the ensemble in phase space is incomplete. The classical coherence—the lock-step motion of the localized trajectory ensemble through phase space—is lost only after several vibrational periods of the newly recombined molecule, when momentum exchange between molecular and bath degrees of freedom becomes sufficiently effective to delocalized the ensemble in phase space. This behavior is quite clearly described by the classical dynamics. What should also be clear is that the pump–probe experiments reflect the classical dynamics rather accurately.

The nearly quantitative reproduction of the envelope of the experimental transient by the single surface simulations implies conservation of flux on the probed surface throughout the observation period. This, in turn, implies that the observed dynamics of dissociation and recombination remains electronically adiabatic, proceeding entirely on the A/A' surfaces. This is in sharp contrast with liquid phase studies, where it has been amply demonstrated that a significant fraction of recombination events proceeds on the X surface.[3] Evidence for recombination on the X surface has also been given in the Ar cluster studies.[6] The anisotropy of I–Rg pair interactions,[33] initial cage/molecule orientation, the extent of interatomic separation at recoil, and the suddenness of the first recoil are the factors that control the adiabaticity of the recombination process.[25,34] A careful assessment of the roles of these different factors in bringing the contrast between the highly constrained dynamics in the solid state vs those in liquid and small cluster environments, would be worthwhile. It is nevertheless clear that very different electronic configurations are reached in the direct recombination channel vs those that involve cage exit and reentry. In the latter case, the convergence of $A/A'(\Pi)$ and $X(\Sigma)$ surfaces is reached with nearly thermalized trajectories, while in the former we can conclude that this does not occur. With respect to the interplay between the A and A' nested potentials, the present experiments yield almost no information.

Finally, we note that although they have not been extended to wavelengths as long as in the present study, experiments nearly identical to the ones reported here, have been performed on I_2 in Ar clusters[6] and in liquid CCl_4.[7] A fast recursion in the pump–probe signal, which has been associated with direct recombination, is observed in those measurements. However, subsequent oscillations are washed out. The rigorous interpretation of those transients requires the establishment of probe resonances, which depend on the solvation of the ion-pair states and may therefore be sensitive to cluster size. Without size resolution, the dispersion in recoil events and probe resonances may preclude the possibility of observing coherences. For neutral species in liquids, the persistence of coherence through the photodissociation-recombination process is not expected, and has not been seen.[7,8] The present dynamics is more comparable to that of I_2^- in size selected clusters, in which vibrational coherence is retained in the recombination process.[5]

VII. CONCLUSIONS

We have reported the direct monitoring of the caging of dissociatively pumped I_2 in solid Kr. Upon preparation of the molecule at energies of 0.15 eV above dissociation: (i) the molecule stretches and the atoms collide with the cage at $t=350\pm50$ fs at an I–I distance of 4.4–4.8 Å; (ii) the recoiling atoms, after losing nearly all of their excess energy, return to the original equilibrium configuration at $t\sim1$ ps; (iii) the nascent I_2 subsequently undergoes 4–5 classical oscillations, with a period of ~0.5 ps, prior to complete loss of coherence. Each of these steps has its direct and unique signature in the experimental pump–probe signals. These features can be well reproduced by classical molecular dynamics simulation, using the classical Franck approximation for pump and probe transitions. It was also shown that for a proper interpretation of ultrafast pump–probe measurements, a good understanding of the transition resonances is crucial. Noting that the many-body potentials required for the treatment of condensed phase data are generally not available, it becomes obvious that iteration between simulation and experiment may be the only viable method for developing a molecular level understanding of condensed phase reactive dynamics. Such an approach was followed in the present work, and a rather detailed interpretation of the experimental observables, together with physical insights relating to the dynamics of breaking and remaking of the I–I bond, could be derived using primitive pair potentials. As more extensive, and more detailed data become available, the obvious next step in refinement of such treatments would be the systematic construction and testing of many-body potentials. For the present case, the serious challenge will be the reliable treatment of the ion-pair states.

While generally similar, there are important differences between the photodissociation dynamics of I_2 in Kr and those reported earlier for I_2 in Ar.[11] The most noticeable of these differences are in the description of the atom-cage collision, which is controlled by the mass asymmetry between guest and host atoms, and which leads to significantly more coherence in the dynamics of the recombinant molecule in Ar. Recent measurements, with an improved time resolution of 150 fs, show that in Ar the coherences persist for as long as the transients are visible—for time periods of ~10 ps. This enables a frequency analysis of the pump–probe signal, and directly yields the lattice motions coupled to the I–I coordinate. Preliminary reports of these observations already exist.[35] A more complete discussion, with a detailed comparison between the different rare gases, is deferred to a future publication.

ACKNOWLEDGMENTS

V.A.A. acknowledges support by AFOSR, under a University Research Initiative Grant No. F49620-1-0251. C.C.M. acknowledges support from the National Science Foundation and the Office of Naval Research. The UCI Office of Academic Computing is acknowledged for an allocation of computer resources.

[1] J. Franck and E. Rabinowitch, Trans. Far. Soc. **30**, 120 (1934).
[2] M. Chergui and N. Schwentner, Trends Chem. Phys. **2**, 89 (1992).
[3] A. L. Harris, J. K. Brown, and C. B. Harris, Ann. Rev. Phys. Chem. **39**, 341 (1988).
[4] J. Schroeder and J. Troe, Ann. Rev. Phys. Chem. **38**, 163 (1987).
[5] J. M. Papanikolas, V. Vorsa, M. E. Nadal, P. J. Campagnola, J. R. Gord, and W. C. Lineberger, J. Chem. Phys. **97**, 7002 (1992); **99**, 8733 (1993).
[6] Q. Liu, J. Wang and A. H. Zewail, Nature, **364**, 427 (1993); E. D. Potter, Q. Liu and A. H. Zewail, Chem. Phys. Lett. **200**, 605 (1992).
[7] A. H. Zewail, M. Dantus, R. M. Bowman, and A. Mokhtari, J. Photochem. Photobiol. A **62**, 301 (1992).
[8] B. J. Schwartz, J. C. King, J. Z. Zhang, and C. B. Harris, Chem. Phys. Lett. **203**, 503 (1993).
[9] J. C. Alfano, D. A. V. Kliner, A. E. Johnson, N. E. Levinger, and P. F. Barbara, in *Ultrafast Phenomena VIII*, edited by J. L. Martin, A. Migus, G. A. Mourou, A. H. Zewail (Springer, New York, 1992), p. 653.
[10] Ch. Lienau and A. H. Zewail, Chem. Phys. Lett. **222**, 224 (1994).
[11] R. Zadoyan, Z. Li, P. Ashjian, C. C. Martens, and V. A. Apkarian, Chem. Phys. Lett. **218**, 504 (1994).
[12] R. Zadoyan and V. A. Apkarian, Chem. Phys. Lett. **206**, 475 (1993).
[13] I. Benjamin, U. Banin, and S. Ruhman, J. Chem. Phys. **98**, 8337 (1993); U. Banin, and S. Ruhman, *ibid.* **98**, 4391 (1993); **99**, 9318 (1993); U. Banin, R. S. Kosloff, and S. Ruhman, Israel J. Chem. **33**, 141 (1993).
[14] D. A. V. Kliner, J. C. Alfano, and P. F. Barbara, J. Chem. Phys. **98**, 5375 (1993).
[15] N. Pugliano, D. K. Palit, A. Z. Szarka, and R. M. Hochstrasser, J. Chem. Phys. **99**, 7273 (1993).
[16] (a) N. F. Scherer, D. M. Jonas, and G. R. Fleming, J. Chem. Phys. **99**, 153 (1993); N. F. Scherer, L. D. Ziegler, and G. R. Fleming, *ibid.* **96**, 5544 (1992).
[17] Y. J. Yan and S. Mukamel, Phys. Rev. A **41**, 6485 (1990).
[18] H. Metiu and V. Engel, J. Chem. Phys. **93**, 5693 (1990).
[19] M. Gruebele and A. H. Zewail, **98**, 883 (1993).
[20] T. J. Smith, L. W. Ungar, and J. A. Cina, J. Lumin. **58**, 66 (1994).
[21] See the series of papers by E. J. Heller, J. Chem. Phys. **62**, 1544 (1975); **65**, 4975 (1976); **68**, 2066, 3891.
[22] J. Franck, Trans. Far. Soc. **21**, 536 (1925).
[23] W. G. Lawrence and V. A. Apkarian, J. Chem. Phys. **101**, 1820 (1994).
[24] A. V. Danilychev and V. A. Apkarian, J. Chem. Phys. **100**, 5556 (1994).
[25] I. H. Gersonde and H. Gabriel, J. Chem. Phys. **98**, 2094 (1993).
[26] A. I. Krylov, R. B. Gerber, and V. A. Apkarian (unpublished).
[27] W. F. Howard and L. Andews, J. Raman Spectrosc. **2**, 447 (1974).
[28] M. Macler and M. Heaven, Chem. Phys. **151**, 219 (1991).
[29] J. Tellinghuisen, J. Mol. Spec. **94**, 231 (1982).
[30] R. Bohling, J. Langen, and U. Schurath, Chem. Phys. **130**, 419 (1989).
[31] J. P. Bergsma, P. H. Berens, K. R. Wilson, D. F. Fredkin, and E. Heller, J. Phys. Chem. **88**, 612 (1984).
[32] G. Kittel, *Introduction to Solid State Physics*, 5th Ed. (Wiley, New York, 1976).
[33] P. Casavecchia, G. He, R. K. Sparks, and Y. T. Lee, J. Chem. Phys. **77**, 1878 (1982).
[34] M. G. Sceats Chem. Phys. **96**, 299 (1985); J. M. Dawes and M. G. Sceats, *ibid.* **96**, 315 (1985).
[35] R. Zadoyan, Z. Li, C. C. Martens, and V. A. Apkarian, SPIE Proceedings **2124**, 233 (1994); in *Ultrafast Phenomena VII*, edited by G. A. Mouron and A. H. Zewail (Springer, New York, to be published).